Published in final edited form as:

ACS Chem Neurosci. 2020 November 18; 11(22): 3802–3813. doi:10.1021/acschemneuro.0c00577.

In Vivo Photopharmacology Enabled by Multifunctional Fibers

James A. Frank◆,
Research Laboratory of Electronics and McGovern Institute for Brain Research, Massachusetts Institute of Technology, Cambridge, Massachusetts 02139, United States; Vollum Institute, Oregon Health & Science University, Portland, Oregon 97239, United States

Marc-Joseph Antonini◆,
Research Laboratory of Electronics and McGovern Institute for Brain Research, Massachusetts Institute of Technology, Cambridge, Massachusetts 02139, United States; Harvard/MIT Health Science & Technology Graduate Program, Cambridge, Massachusetts 02139, United States

Po-Han Chiang,
Research Laboratory of Electronics, Massachusetts Institute of Technology, Cambridge, Massachusetts 02139, United States; Institute of Biomedical Engineering, National Chiao Tung University, Hsinchu 300, Taiwan (R.O.C.)

Andres Canales,
Research Laboratory of Electronics and Department of Materials Science and Engineering, Massachusetts Institute of Technology, Cambridge, Massachusetts 02139, United States

David B. Konrad,
Department of Pharmacy, Ludwig Maximilian University, D-81377 Munich, Germany

Indie C. Garwood,
Research Laboratory of Electronics and McGovern Institute for Brain Research, Massachusetts Institute of Technology, Cambridge, Massachusetts 02139, United States; Harvard/MIT Health Science & Technology Graduate Program, Cambridge, Massachusetts 02139, United States

Gabriela Rajic,

Corresponding Authors: **Polina Anikeeva** – Research Laboratory of Electronics, McGovern Institute for Brain Research, and Department of Materials Science and Engineering, Massachusetts Institute of Technology, Cambridge, Massachusetts 02139, United States; anikeeva@ mit.edu; **James A. Frank** – Research Laboratory of Electronics and McGovern Institute for Brain Research, Massachusetts Institute of Technology, Cambridge, Massachusetts 02139, United States; Vollum Institute, Oregon Health & Science University, Portland, Oregon 97239, United States; frankja@ohsu.edu.

◆Author Contributions

J.A.F. and M.J.A. contributed equally to this work.

Author Contributions

J.A.F. and P.A. conceived and coordinated the study. D.B.K. synthesized the photoswitchable compounds. J.A.F. and G.R. carried out imaging experiments in cultured neurons. J.A.F., M.J.A., and I.G. fabricated and characterized the multifunctional fibers. Y.F. aided in fiber design. P.C. and F.K. produced lentiviral vectors. J.A.F., M.J.A., P.C., A.C., and I.G. performed immunohistochemical experiments. J.A.F. and M.J.A. performed the behavioral experiments. P.C., A.C., M.J.A., and J.A.F. wrote scripts for data analysis. J.A.F., M.J.A., and P.A. wrote the manuscript with input from all coauthors.

Supporting Information

The Supporting Information is available free of charge at https://pubs.acs.org/doi/10.1021/acschemneuro.0c00577.

Figure S1, *red*-AzCA vehicle control experiments in cultured neurons; Figure S2, drawing parameters and thermal drawing process; Figure S3, fiber connectorization process; Figure S4, implantation locations; Figure S5, chemogenetic control of VTA projections; and Table S1, corresponding primary and secondary antibodies for immunohistochemistry (PDF)

Complete contact information is available at: https://pubs.acs.org/10.1021/acschemneuro.0c00577

The authors declare no competing financial interest.

Vollum Institute, Oregon Health & Science University, Portland, Oregon 97239, United States

Florian Koehler,
Research Laboratory of Electronics and Department of Electrical Engineering and Computer Science, Massachusetts Institute of Technology, Cambridge, Massachusetts 02139, United States

Yoel Fink,
Research Laboratory of Electronics and Department of Materials Science and Engineering, Massachusetts Institute of Technology, Cambridge, Massachusetts 02139, United States

Polina Anikeeva
Research Laboratory of Electronics, McGovern Institute for Brain Research, and Department of Materials Science and Engineering, Massachusetts Institute of Technology, Cambridge, Massachusetts 02139, United States

Abstract

Photoswitchable ligands can add an optical switch to a target receptor or signaling cascade and enable reversible control of neural circuits. The application of this approach, termed photopharmacology, to behavioral experiments has been impeded by a lack of integrated hardware capable of delivering both light and compounds to deep brain regions in moving subjects. Here, we devise a hybrid photochemical genetic approach to target neurons using a photoswitchable agonist of the capsaicin receptor TRPV1, *red*-AzCA-4. Using multifunctional fibers with optical and microfluidic capabilities, we delivered a transgene coding for TRPV1 into the ventral tegmental area (VTA). This sensitized excitatory VTA neurons to *red*-AzCA-4, allowing us to optically control conditioned place preference in mice, thus extending applications of photopharmacology to behavioral experiments. Applied to endogenous receptors, our approach may accelerate future studies of molecular mechanisms underlying animal behavior.

Graphical Abstract

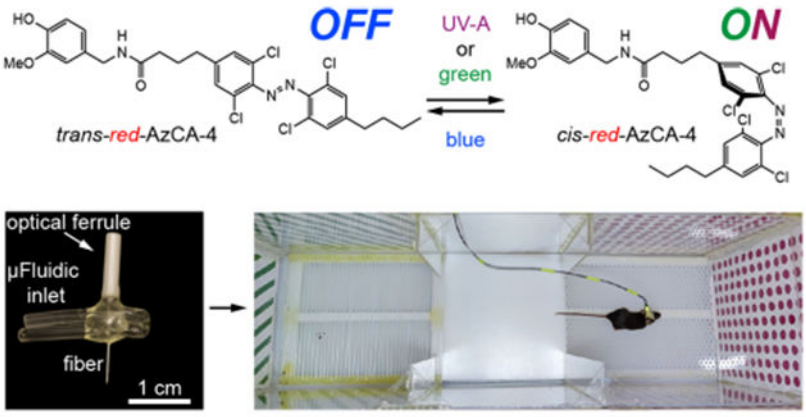

Keywords

Photopharmacology; fibers; chemical genetics; capsaicin; TRPV1; neural probes

INTRODUCTION

To illuminate the molecular mechanisms underlying neuronal function, a number of chemical and genetic techniques have been developed to place cells under optical control.[1–3] As demonstrated by optogenetics, the enhanced spatiotemporal precision attained using an optical stimulus is enabling to understanding how specific circuits control behavior and animal physiology.[1,4] However, optogenetics has so far relied on exogenously expressed microbial rhodopsins, thus offering a means to investigate electrophysiological, but not molecular, mechanisms underlying neural dynamics and behavior. Light-controllable ligands present an attractive alternative to optogenetics, as they add an optical switch to a pharmacological agent to place cell signaling pathways under optical control.[5] Of particular utility are azobenzene photoswitches, which can be synthetically incorporated into a small-molecule ligand.[6,7] Their activity can then be reversibly tuned using different wavelengths of light *via trans/cis* isomerization. Termed photopharmacology,[8] this approach has been applied to manipulate ion channels, G protein-coupled receptors (GPCRs), enzymes, components of the cytoskeleton, and even cellular membranes.[6,9–14] These photoswitchable small molecules can target endogenous receptors or, alternatively, genetically inserted exogenous proteins to create a wide variety of signaling events.

Since its inception, photopharmacology has been applied to primary culture and tissues (*i.e. Xenopus oocytes*, pancreatic islets, acute brain slices),[15–17] owing to the ease of light delivery. The challenges associated with simultaneous delivery of light in addition to the photoswitchable compounds have largely limited *in vivo* application of photopharmacology to small and transparent model organisms, including zebrafish larvae and *Caenorhabditis elegans*.[18,19] Unfortunately, the utility of photopharmacology for studying mammalian behavior has been hindered by the lack of available hardware for delivering the chemical probes and optical stimuli to nonsuperficial brain regions. Although several recent studies have applied azobenzene-based probes to control behavior in freely moving rodents, they used commercially available devices composed of a guide cannula which houses interchangeable injectors for ligand and light delivery.[20–22] Device exchange may cause subject stress during experiments and obfuscate behavioral assays, and additionally increase the probability of infection or tissue damage. Furthermore, commercial cannulas offer limited options for tailoring of functional features to the scientific question. As such, the development of customizable and integrated hardware that allows both chemical and optical stimulation in deep brain regions of freely moving subjects may facilitate the adoption of photopharmacology by the neuroscience community.

A number of devices permitting concurrent optical and chemical stimulation in the rodent brain have been developed.[23–26] Lithography-based microfabrication has emerged as a powerful technique to produce tethered and wireless multifunctional neural implants.[24,26–31] However, their dissemination and adoption by the larger neuroscience community has been hindered by high costs and limited scalability. Another strategy, the thermal drawing process (TDP), allows the creation of fiber-based neural implants with multiple functionalities.[25,32,33] During the TDP, a macroscale (centimeters in diameter) preform is fabricated with the same cross-sectional geometry and functional features as the final device. The preform is then heated above the materials' glass transition temperature (T_g)

and stretched to create hundreds of meters of a sub-mm-sized device with preserved cross-sectional geometry. The TDP is compatible with a variety of polymers, glass, and metals, enabling the fabrication of multifunctional fibers that can feature microfluidic channels, optical waveguides, and electrodes. From a single preform that is typically 20–30 cm long, the TDP can yield hundreds of neural implants, making it a cost-efficient and scalable alternative to microfabrication.[34] Additionally, these devices are versatile in terms of functionality and can be customized to suit the particular needs of any given experiment. Although the TDP has been used to create implants for targeting the brain and spinal cord,[25,32,33] to date they have not been combined with photopharmacology to manipulate neuronal function.

In this study, we devise a photochemical genetic method to manipulate neural circuits using the photoswitchable capsaicin (CAP) analog, *red*-AzCA-4.[35] To translate this approach from cell culture to behavioral experiments, we used the TDP to create a flexible multifunctional fiber that can deliver optical and chemical stimulation to deep brain regions in mice. We targeted the ventral tegmental area (VTA), a midbrain region involved in dopaminergic reward signaling, by injecting a virus coding for the transient receptor potential vanilloid family member 1 (TRPV1, capsaicin receptor) under the CaMKIIα promoter. This sensitized excitatory neurons to *red*-AzCA-4, which could manipulate conditioned place preference behavior in freely moving mice in a light-dependent manner. This proof-of-concept study illustrates how multifunctional fiber-based neural probes can be used to translate the use of chemical photoswitches from *in vitro* studies to behavioral experiments *in vivo*. Our approach is flexible and modular and can be used to target a wide variety of cellular signaling systems through multiple modalities. This sets the stage for new applications of photopharmacology in manipulating neural circuits *in vivo* to unveil molecular mechanisms underlying behavior.

RESULTS AND DISCUSSION

Optical Control of TRPV1-Expressing Neurons Using *red*-AzCA-4.

We previously developed photoswitchable CAP analogs that can optically control TRPV1, a nonselective cation channel which is expressed primarily in nociceptive neurons.[36,37] The first generation probe, AzCA-4,[38] includes an azobenzene photoswitch that can be isomerized between the *cis/trans* forms with UV-A/blue light, respectively. AzCA-4 possessed a greater efficacy toward TRPV1 in the *cis*-form, and isomerization could reversibly control endogenously expressed TRPV1 in sensory neurons *in vitro* and *ex vivo*. However, due to the phototoxicity and poor tissue penetration of UV-A (350–380 nm) irradiation required to generate the *cis*-isomer, AzCA-4 was not suitable for applications *in vivo*. A red-shifted derivative, *red*-AzCA-4,[35] which possesses four chlorine atoms at the *ortho*-positions of the azobenzene moiety (Figure 1A), was designed to isomerize to the more potent *cis*-form with green (500–590 nm) as well as the UV-A light, while returning to the *trans*-form upon exposure to blue light (410–480 nm). This increases its applicability toward experiments in intact tissue, as longer wavelength visible light is less phototoxic.[39,40] Although *red*-AzCA-4 was shown to behave similarly to AzCA-4

in cultured cells heterologously expressing TRPV1, its utility in modulating activity of TRPV1-expressing neurons *in vitro* and *in vivo* remained unexplored.

To sensitize neurons to CAP and *red*-AzCA-4, we utilized a lentivirus carrying the TRPV1 transgene under the excitatory neural promoter calmodulin kinase II α-subunit (CaMKIIα). TRPV1 expression was linked to a red fluorescent protein mCherry by a post-transcriptional cleavage linker p2A[41] (Lenti-CaMKIIα::TRPV1-p2A-mCherry).[42] In primary rat neurons, lentiviral transduction affected nearly 100% of the cells as marked by colocalization of mCherry expression with neuronal marker NeuN (Figure 1B).[43] To test the activity of *red*-AzCA-4 on transduced neurons, the culture was incubated with the Ca^{2+}-sensitive dye Fluo-4-AM, and the intracellular Ca^{2+} concentration ($[Ca^{2+}]_i$) was monitored using confocal fluorescence imaging. To enable simultaneous imaging of the green Fluo-4 fluorescence during photoswitching, *red*-AzCA-4 was isomerized to the *cis*-form using a 375 nm (UV-A) quenching laser. No fluorescence increase was observed on addition of the *trans*-compound; however, irradiation with a 375 nm laser caused a rapid increase in Fluo-4 fluorescence, demonstrating that *cis-red*-AzCA-4 increased the $[Ca^{2+}]_i$ (Figure 1C–E). In control experiments, addition of CAP also caused an increase in $[Ca^{2+}]_i$ which decayed over time due to TRPV1 desensitization (Figure S1A,B). Additionally, UV-A irradiation alone or a vehicle addition (0.1% DMSO in buffer) ± irradiation did not affect $[Ca^{2+}]_i$ (Figure S1C,D). These results indicate that the *cis*-isomer of *red*-AzCA-4 activates TRPV1 more strongly than the *trans*-isomer, which is consistent with the results obtained in previous studies.[35,38]

Developing a Multifunctional Fiber for *in Vivo* Photopharmacology.

Fibers capable of optical stimulation alongside chemical/virus delivery were produced via thermal drawing of macroscale preforms (Figure 2A,B). The fibers contained a polymer optical waveguide and two microfluidic channels, which were fabricated out of polycarbonate (PC) and cyclic-olefin-copolymer (COC) (Figure 2C, top). These materials possess similar T_g (PC, T_g = 150 °C; COC, T_g = 158 °C), making them suitable for co-drawing. By tuning the preform feeding and fiber drawing speeds, the cross section of the preform (3.7 × 2.6 cm^2) was reduced to 480 × 340 μm^2 in the final fiber (Figure 2C, middle, Figure S2). Connectorization of the microfluidic channels to ethyl vinyl acetate (EVA) tubing and the PC/COC waveguide to a ceramic optical ferrule (Figure S3) afforded the final implant with light and fluid-delivery capabilities (Figure 2C, bottom). The final device was miniature (2.5 × 2 × 0.5 cm^3) and lightweight (0.82 ± 0.06 g), which permitted unconstrained movement of mice in their home cage following implantation.

We characterized the optical waveguide using fiber-coupled LEDs across the UV–visible range by measuring the optical loss over different lengths of fiber (Figure 2D, left). Optical losses across the visible range spanned 0.67 ± 0.03, 0.42 ± 0.03, 0.48 ± 0.07, 0.41 ± 0.03, and 0.39 ± 0.02 dB/cm for 420, 470, 565, 595, and 620 nm wavelengths, respectively (Figure 2D, right). These values are comparable to those previously obtained in thermally drawn polymer fibers [1.2–2.7 dB/cm].[25,32,33,44] This makes our device suitable for controlling photoswitchable ligands with light across the visible spectrum.[39] Due to the absorbance of PC used as the waveguide core in the UV-A range, the optical loss at 365 nm

was 2.03 ± 0.15 dB/cm. We then tested the microfluidic channels by injecting Trypan blue dye into a “phantom brain”, consisting of 0.6% agarose gel. No leaks were observed along the fiber length, and the fluid delivery did not interfere with optical illumination (Figure 2E). The dead volume within the microfluidic channel of the fiber was 0.36 μL (0.085 × 0.17 × 25 mm^3). The dead volume within the EVA tubing was minimized by inserting a 36g needle all the way until the EVA interfaces with the fiber and by filling the EVA tubing with solution. Thanks to the large difference between the EVA tube lumen and the 36g needle diameter, the air was effectively pushed out of the EVA tubing and replaced by the solution to be injected. Furthermore, fluid return rates were >80% at injection speeds ranging between 10 and 400 nL/s and an efficiency ~60% at 1 nL/s (Figure 2F). The slight decrease in efficiency observed at very low flow rates can likely be explained by the evaporation of water over the duration of the measurement (~2.5 h). Taken together, these results demonstrate that our fibers can concurrently deliver both optical and chemical (fluid) stimuli.

In Vivo Photopharmacology of Mesolimbic Circuitry.

To test the utility of our fibers for delivering and optically actuating photoswitchable ligands to deep brain regions *in vivo*, we implanted our devices into the VTA in mice. The VTA is known as a dopaminergic hub involved in reward signaling and reinforcement learning, and its dopaminergic projections to the nucleus accumbens (NAc) and medial prefrontal cortex (mPFC) are well characterized.[45–47] The fibers were used to deliver Lenti-CaMKIIα::TRPV1-p2A-mCherry virus (1.5 μL >10^{10} particles/mL) into the VTA during the implantation surgery (Figure 3A,B). This one-step surgery reduces the tissue damage that may occur during multiple surgeries and also ensures colocalization of the expression profile with the optical and pharmacological interrogation volume.[32] Six to eight weeks post-implantation, we confirmed TRPV1 expression and the fiber position in the VTA (Figures 3C and S4).[48,49]

Next, we tested the ability of CAP and *red*-AzCA-4 to activate transduced TRPV1-expressing VTA neurons *in vivo* by quantifying the expression of c-Fos.[50] This immediate early gene serves as a marker of neuronal activity, as its expression and translocation to the nucleus are upregulated in recently activated neurons.[51] A separate cohort of mice received a Lenti-CamKIIα::mCherry virus as a negative control. CAP or *red*-AzCA-4 were injected through the microfluidic channels of the implanted fibers over 5 min concurrently with illumination. We showed that CAP injection (10 μM) into TRPV1-expressing mice (N = 7) caused an increase in c-Fos expression in the VTA when compared to those only expressing mCherry (N = 7) (Figure 3D,E). The locations of the c-Fos expressing cells correlated with the region displaying mCherry fluorescence. Next, *red*-AzCA-4 (1 μM) was injected under either 420 or 565 nm illumination. We observed a greater c-Fos expression in the VTA in the presence of green light (N = 7) compared to blue light (N = 5), indicating that *cis-red*-AzCA-4 activates VTA neurons more strongly than the *trans*-isomer (Figure 3D,F). c-Fos immunofluorescence imaging in the NAc and mPFC also revealed greater c-Fos expression in response to *cis-red*-AzCA-4 compared to *trans-red*-AzCA-4 (Figure S5). Consistent with prior work, these results demonstrate that multifunctional fibers are capable of delivering viruses, chemicals, and light to deep brain regions. Notably, both CAP and

red-AzCA-4 activate sensitized neurons, where *red*-AzCA-4 affords an additional level of optical control. As such, our approach is suitable for photopharmacological manipulation of neural circuits *in vivo*.

Optical Control of Place Preference Using *red*-AzCA-4.

Activation of the mesolimbic pathway is associated with rewarding/salient stimuli and is known to drive behavioral preference in mice.[52] To test the ability of *red*-AzCA-4 to activate the mesolimbic pathway in a light-dependent manner, we performed a three-chamber conditioned place preference (CPP) assay.[53] Mice were implanted with multifunctional fibers and concomitantly injected with a Lenti-CaM-KIIα::TRPV1-p2A-mCherry into the VTA, and the CPP assay was performed six to eight weeks post-implantation. Mice injected with Lenti-CaMKIIα::mCherry served as negative controls. The first day of the CPP protocol began with a 45 min pretest during which each mouse could freely explore a three-chambered arena. The left and right chambers were distinguishable by patterns on the floor and walls (holes vs bars) (Figure 4A). On the second and third conditioning days, the mice were confined to a single chamber where they received unique chemical and optical stimulation. Between mice, the stimuli were randomized with respect to the chamber. The fourth day consisted of a post-test where each mouse could explore the entire box. The relative time spent in each chamber was compared between day one (pretest) and day four (post-test) to determine the preference of the mice for the two stimuli. A cohort of mice was conditioned to compare CAP vs vehicle control, while another received *red*-AzCA-4 injections with either blue or green light (Figure 4B). In the pretest, TRPV1-expressing mice displayed no preference for either chamber (p-value = 0.6580, $N = 19$). However, in the post-test, mice spent more time in the chamber in which they received a CAP injection (10 μM) compared to the vehicle control (0.2% DMSO) (p-value = 0.0313, $N = 7$) (Figure 4C,D). Similarly, mice injected with *red*-AzCA-4 (1 μM) preferred the chamber in which they received green (*cis-red*-AzCA-4) compared to blue illumination (*trans-red*-AzCA-4) (p-value = 0.0342, $N = 12$) (Figure 4C,D). Mice expressing mCherry alone did not develop a preference for CAP over the vehicle control (pretest p-value = 0.6406, post-test p-value = 0.7422, $N = 8$) (Figure 4E), indicating that exogenous TRPV1 expression in the VTA is necessary to drive preference. These results are consistent with our *in vitro* studies and c-Fos quantification experiments, where *cis-red*-AzCA-4 activates TRPV1 more potently. These findings confirm that *red*-AzCA-4 combined with the multifunctional fibers enable optical control behavior in freely moving mice.

Since the first azobenzene-based photoswitches were employed to reversibly activate ion channels,[16,54,55] photopharmacology has evolved beyond proof-of-principle. An optical switch can be placed on virtually any pharmacological agent to modulate defined components of the cellular signaling machinery. Although chemical photoswitches have been extensively applied to *in vitro* and in vertebrates,[9] their use in the neuroscience community has lagged primarily due to challenges in applying these probes to mammalian models. Bringing the chemical flexibility of photopharmacology to the neuroscience community is therefore an important step in understanding the molecular mechanisms underlying behavior.

In this study, we demonstrated that photopharmacological manipulation of ion channels affords optical control of neural circuits sufficient to modulate behavior. Our *in vivo* studies show that green light potentiates the effect of the photoswitchable compound *red*-AzCA-4 by generating the more potent *cis*-isomer. Although the *trans*-isomer of *red*-AzCA-4 displays some activity at TRPV1, isomerization is still sufficient to activate reward circuits to drive increased c-Fos expression and preference behavior. Compared to recent applications of *in vivo* photopharmacology in mice which required a separate cannula and waveguide for probe and light delivery,[20–22] our multifunctional device can deliver transgenes, ligands, and light to deep brain regions such as the VTA. We anticipate this will increase the reproducibility of behavioral experiments reliant on photopharmacological manipulation of ion channels. Future studies will aim to develop more compact devices that would further reduce the impact on the surrounding tissue. For example, elastomers or hydrogels could offer low modulus alternatives to the polymers currently comprising photopharmacology probes.[33,56] Our fiber-based probes rely on tethers to the external light and fluid sources. Although prior work on wireless opto-fluidic platforms enabled tetherless operation,[24,57,58] it offered limited flexibility in optical and chemical stimuli following implantation. In contrast, our approach allowed us to easily modify the type, volume, and infusion rate of the delivered fluids as well as the wavelengths of light for photoswitching. Unlike wirelessly powered devices,[57–59] our fibers are compatible with standard behavioral arenas, do not rely on custom antennas for power transmission, and thus, can be readily adopted by neuroscience groups that routinely rely on optogenetics and pharmacology. Finally, thermal drawing permits the integration of additional functional features including electrophysiological recording,[32] which may in the future allow us to observe photopharmacological switching of neuronal activity in real-time. This will permit the direct correlation of photopharmacological ion channel manipulation to the dynamics of local circuits in the context of behavior.

This proof-of-principle study relied on genetic manipulation to introduce the mammalian receptor TRPV1 in the VTA to achieve photopharmacological control of neurons. Our approach is, however, immediately translatable to photoswitchable ligands targeting endogenous proteins. This will enable optical manipulation of neural circuits, or even nonexcitable cells such as glia, without the need for genetic editing. For example, *red*-AzCA-4 could target the naturally expressed TRPV1 in the peripheral nervous system, while other photoswitchable ligands could affect cannabinoid receptors in the brain.[60] Transgene-free optical manipulation of neural circuits is desirable for model organisms beyond mice, where genetic tools are not as readily available. This would also be of significant importance for the development of potential therapeutic applications, where genetic manipulation still remains a significant barrier.

The advent of optogenetics revolutionized how neuroscientists dissect neural circuitry, yet it remains limited to manipulation of electroactive cells via triggering ion transport through microbial proteins. Photopharmacology empowered by integrated multifunctional fibers will permit direct manipulation of endogenous receptors within living organisms. This will facilitate studies of the roles of specific neurotransmitters and effector pathways in driving the neural circuits that dictate behavior, physiology, and pathology.

METHODS

Materials Availability.

If available, *red*-AzCA-4 and fibers can be provided from the authors but may require completion of a Materials Transfer Agreement.

Data and Code Availability.

The data sets supporting the current study are freely available from the corresponding author on request. All MATLAB and python codes used for data analysis are available on request.

Experimental Models and Subject Details.

Animals.—Primary neuronal culture experiments were performed in accordance with the IACUC protocol IP00002121 (optical tools for controlling and recording neurotransmission). These used primary hippocampal neurons from male and female neonatal wild-type Sprague–Dawley rats (Charles River, Crl:CD, 8–12 pups, P0–P1).

All stereotactic surgeries for *in vivo* experiments were performed in accordance with the IACUC protocol 0118-003-21 (Implantation of Neural Recording and Stimulation Devices into Adult Mice and Rats). These were performed using 8-week-old male BL6C/57 mice (Jackson, BL6C/57, #000664). Mice were housed in a normal 12-h light/dark cycle and fed a standard rodent chow diet. After device implantation, mice remained single-housed and were not used for experiments if they experienced symptoms of decreased health.

Chemical Reagents and Synthesis.

All reactions were magnetically stirred under inert gas (N_2) atmosphere using standard Schlenk techniques. Glassware was evacuated and dried by heating with a heat-gun (set to 550 °C). Drying over Na_2SO_4 implies stirring with excess anhydrous salt for 3–5 min followed by filtration through a glass frit and rinsing of the filter cake with additional solvent. Cannulas and syringes which were used for transferring reagents or solvents were flooded with inert gas (3×) before use. Purification by column chromatography was performed under elevated pressure (flash column chromatography) on Geduran© Si60 silica gel (40–63 μm) from Merck KGaA. After flash column chromatography, the concentrated fractions were filtered once through a glass frit. Silica gel F_{254} TLC plates from Merck KGaA were used for monitoring reactions, analyzing fractions of column chromatography and measuring R_f values. Drying via lyophilization or freeze-drying refers to freezing of the respective sample in liquid nitrogen followed by evacuating the containing flask with high vacuum (<1 mbar) and slow thawing to room temperature. Reaction yields refer to spectroscopically pure isolated amounts of compounds. NMR spectra were acquired on a Bruker Avance III HD 400 with Cryo-head (400 MHz for ^1H and 101 MHz for ^{13}C spectroscopy). High-resolution mass spectra were recorded on a Thermo Finnigan LTQ FT (ESI: electrospray ionization).

Unless otherwise specified, chemicals were purchased from *Sigma-Aldrich, Fisher Scientific, TCI Europe, Chempur, Alfa Aesar*, or *Acros Organics*. Solvents purchased in technical grade quality were distilled under reduced pressure and used for purification

procedures. Triethylamine (NEt_3) was dried by distillation from CaH_2. Dry EtOAc was purchased from commercial sources (*Acros Organics*, *Fisher Scientific*) under inert gas atmosphere and over molecular sieves. All other reagents with a purity of >95% were purchased from commercial sources and used without further purification. *red*-FAAzo-4 was synthesized according to our literature procedure.[35] The large-scale synthesis of *red*-AzCA-4 is as follows:

Synthesis of *red*-AzCA-4.

red-FAAzo-4 (700 mg, 1.48 mmol, 1.00 equiv) was placed in a Schlenk flask and freeze-dried (2 cycles). 2-(1H-Benzotriazole-1-yl)-1,1,3,3-tetramethylaminium tetrafluoroborate (TBTU, 476 mg, 1.48 mmol, 1.00 equiv) was added, and the mixture was dissolved in EtOAc (59.3 mL). After a dropwise addition of NEt_3 (0.62 mL), the red solution was stirred for 70 min at room temperature. Vanillylamine hydrochloride (562 mg, 2.96 mmol, 2.00 equiv) was added in one portion, and stirring was continued at room temperature for 2 h. The solution was diluted with EtOAc (250 mL) and washed with 3% $KHSO_4$ (50 mL) and saturated aqueous NaCl (100 mL) followed by drying over Na_2SO_4 and removal of the solvent *in vacuo*. Two consecutive column chromatography steps (pentane:EtOAc = 1:1) afforded *red*-AzCA-4 (740 mg, 1.24 mmol, 84%) as a dark red solid. The analytical data is in accordance with those reported in the literature.[35]

Cell Culture Media and Solutions.

Dissection Solution.—This solution contains (in mM) 160 NaCl, 5 KCl, 0.5 $MgSO_4$, 3 $CaCl_2$, 5 HEPES, and 5.5 glucose with 2.0 mg/L phenol red. The pH was adjusted to 7.4 with NaOH, and the solution was sterile filtered and aliquoted.

Enzymatic Solution.—This solution contains dissection solution (10 mL), L-cysteine (2 mg), EDTA (25 mM, 200 μL aliquot), $CaCl_2$ (100 mM, 100 μL aliquot), NaOH (1 N, 30 μL), DNase (0.05 mg/mL, Sigma, DN25), and papain (100 μL, Sigma, P3125).

Serum Media.—This solution contains minimum essential medium (MEM, 500 mL, with Earle's salts, without glutamine), Glutamax (5 mL, Gibco), fetal bovine serum (FBS, 25 mL), and MITO+ serum extender (1 mL, Corning, 35506, diluted 3× in H_2O) and was sterile filtered and aliquoted.

Inactivation Solution.—This solution contains serum media (10 mL), bovine albumin (25 mg), soybean trypsin inhibitor (25 mg, Gibco, 17075-029), and DNase I (0.05 mg/mL, Sigma, DN25).

Neurobasal A+ Media.—This media contains Neurobasal-A medium (500 mL, Gibco), B-27 supplement (20 mL, Gibco), Glutamax (5 mL, Gibco), and FBS (15 mL) and was sterile filtered and aliquoted.

FUDR inhibitor.—This inhibitor contains uridine (5 mg/mL) and 5-fluorodeoxyuridine (2 mg/mL) in MEM (with Earle's salts, without glutamine) and was sterile filtered and aliquoted.

Imaging Buffer.—This buffer contains (in mM) 115 NaCl, 1.2 $CaCl_2$, 1.2 $MgCl_2$, 1.2 K_2HPO_4, 20 HEPES, and 20 D-glucose and was adjusted to pH 7.4 with NaOH, sterile filtered, and aliquoted.

Primary Rat Hippocampal Culture.

The day before the culture, glass-bottom 8-chamber μ-slides (Ibidi, 80827) were coated with poly-L-lysine (PLL, 50 μL per well) and incubated at 37 °C for 25 min. The chambers were washed with phosphate-buffered saline (PBS, 1x, pH 7.4) and dried for 25 min at 37 °C. The chambers were then coated with mouse laminin (50 μL per well, ≈15 ng/mL in PBS, Corning, 354232) and incubated overnight at 37 °C. Neonatal wild-type Sprague–Dawley rats (Charles River, Crl:CD, 8–12 pups, P0-P1) were anesthetized on ice and quickly euthanized by decapitation. The hippocampi were quickly dissected in cold dissection solution and then transferred to sterile filtered enzymatic solution (10 mL) in which they were incubated at 37 °C for 25 min. The hippocampi were then transferred to a sterile filtered inactivation solution (10 mL) at room temperature for 2 min. All but ≈1 mL of the media was removed by aspiration, and the neurons were gently triturated with a 200 μL pipet until a homogeneous cloudy solution was achieved. The dissociated cells were diluted in serum media (1 mL per hippocampus) and then counted (30 μL cells w/10 μL Trypan blue). The cells were plated into the PLL/laminin-coated lab-tecs (200,000 cells/chamber) and cultured at 37 °C in 5% CO_2. 36–48 h later, the media was exchanged for Neurobasal A+ media (220 μL/chamber), and 30 μL of FUDR inhibitor solution was added to each well. Neurons were infected with lentivirus (1:2250× dilution of $>10^{10}$ particles/mL concentrated virus in Neurobasal A+ media) at DIV5. Every 3 days the media was exchanged for fresh Neurobasal A+ media (250 μL/chamber).

Fiber Fabrication.

The neural implant was fabricated by using the thermal drawing process on a macroscopic template (preform). To fabricate the preform, we rolled several cyclic-olefin-copolymer (COC 6015; TOPAS) and polycarbonate sheets (PC; Ajedium films) onto a 12.7 mm PC rod (McMaster) to reach a 16.4 mm diameter assembly and consolidated under vacuum at 175 °C for ≈30 min, forming a single solid COC/PC preform. Two PC slabs (35.45 × 15 × 200 mm; McMaster) were machined to have one semicircular channel (16.5 mm diameter; 200 mm length), and two rectangular grooves (6.35 × 6 × 200 mm) were machined on each side of the semicircular channel. Two aluminum (Al) slabs (McMaster) were milled to form 11.75 × 5.75 × 200 mm^3 bars, around which several fluorinated ethylene propylene (FEP) films (McMaster) were rolled to form a 12 × 6 × 200 mm^3 spacer, which was placed inside the rectangular groove and sandwiched between the PC slabs prior to consolidation.

The COC/PC preform was then consolidated in a hot press at 175 °C for 1 h at 1000 psi. Finally, additional PC sheets were wrapped around the overall assembly to provide additional support, and the whole assembly was again consolidated under vacuum at 175 °C for 30 min. The resulting preform was then drawn at 300 °C using a custom-built fiber drawing tower as described in previous work.[25,32]

Fiber Connectorization.

The connectorization process is depicted in Figure S3. Drawn fiber was cut to length (4 cm for implantation devices), and one end was coated with epoxy (Devcon, 14250) to protect the polycarbonate (PC) waveguide. The outer PC housing was etched away from the top 1.5 cm of the fiber by submerging the tip in CH_2Cl_2 for 2 min. After removal of the epoxy tip, the COC/PC waveguide was glued (Devcon epoxy, 14250) into a ceramic ferrule (ThorLabs, CF270) and left to dry overnight. The microfluidic channels were each opened below the ferrule using a scalpel, and the fiber was inserted through two pieces of ethyl vinyl acetate (EVA) tubing (0.03″ ID, 0.09″ OD, McMaster-Carr, 1883T2), with the core of each tube overlapping the openings for the microfluidic channels. One end of each tube and the region in contact with the fiber was sealed with epoxy (Devcon, 14250), and the ferrule was polished using fiber polishing film (ThorLabs) as described by the manufacturer.

Microinjection and Optical Stimulation.

Fibers were connected to a Nanofil syringe (10 μL, World Precision Instruments) using a home-built connector consisting of a Nanofil beveled needle (33G, World Precision Instruments, NF33BV), EVA tubing (0.03″ ID, 0.09″ OD, McMaster-Carr, 1883T2), and dispensing needle (19G, McMaster-Carr, straight: 75165A554, or 90°: 75165A66). The individual components were assembled and sealed with 5-min epoxy (Devcon, 14250). Injections were controlled using a syringe pump (World Precision Instruments, Micro4, UMC4) and controller (World Precision Instruments, UMP3).

Optical stimulation was generated using fiber-coupled LEDs (Thorlabs, M420F2, M565F3) driven by an LED driver (Thorlabs, LEDD1B, 0.6 A current limit) and a waveform generator (Agilent 33500B). LEDs were coupled to the ferrule on the device using a rotary joint optical fiber (Thorlabs, RJPSF2) and a ceramic mating sleeve (Thorlabs, ADAF1).

Microfluidic Characterization - Phantom Brain Injection and Injection Efficiency.

Agarose gel (Sigma) was dissolved in distilled H_2O (0.6 wt %/vol) with gentle microwave heating, poured into a 2 mL glass vial, and allowed to cool overnight. The fiber tip was inserted into the agarose gel, and the injection was driven using a syringe pump (WPI Micro4, UMC4) and controller (WPI, UMP3), via a Hamilton syringe and EVA tubing (McMaster, #1883T1). Trypan blue (3 μL) was injected at a speed of 100 nL/min. Images were captured using a Nikon D610 digital single-lens reflex camera and a 100 mm macro lens (Tokina). RAW images were processed in Adobe Photoshop, where corrections were applied only to increase sharpness and color contrast.

To further characterize the microfluidic capabilities of the neural implant, the microfluidic inlet of the device was connected to the injection apparatus described above (Nanofil, syringe pump, and controller). We injected water (9 μL) into a phantom brain at target injection rates of 1, 20, 50, 80, 100, 200, and 400 nL/s through the microfluidic channel, and the injection output was measured by weight. The output injection rate was calculated by dividing the injection output by the time required to inject it. Injection efficiency was calculated by comparing input and output injection rates.

Optical Loss Calculation.

To calculate the optical loss, fibers (11 cm in length) were etched and connected to a ferrule (ThorLabs, CF270) as described above. The fiber was connected to fiber-coupled LEDs (Thorlabs, M365FP1, M420F2, M470F3, M565F3, M595F2, M625F2) using a rotary joint optical fiber (Thorlabs, RJPSF2) and a metal interconnect (Thorlabs, ADAF2). The absolute output power was measured using a digital power meter (Thorlabs, PM100D) with a photodiode power sensor (Thorlabs, S121C). Two cm sections of fiber were then removed, and the power at each length was measured down to 1 cm. The recorded power values at each length were normalized to the power at the shortest length. This procedure was repeated for multiple fibers, and the normalized powers were averaged and plotted (Figure 2D). The decibel loss was calculated across each cut section as

$$\text{Optical Loss} = \frac{10}{L} \times \log\left(\frac{P_{\text{in}}}{P_{\text{out}}}\right)$$

in dB/cm, where L = fiber length in cm, P_{in} = input power in mW, and P_{out} = output power in mW. The values across the 11 cm segments of each fiber were averaged, and the error was calculated as ± SEM.

Lentivirus Packaging.

Plasmids for lentivirus packaging were amplified by transformation into stellar competent cells (ClonTech) and extracted with an endotoxin-free maxi-prep DNA extraction kit (Qiagen). Lenti-X HEK 293T cells (ClonTech) were used for producing lentiviral particles and were maintained in a 10 cm Petri dish (Corning) in DMEM with 10% FBS (Thermofisher) without an antibiotic for >3 passages before transfection. Cells were transfected with the third generation lentivirus and helper plasmids when the cells reached 80–90% confluence. Before transfection, HEK cells were incubated in 6 mL of fresh and prewarmed DMEM with 10% FBS for 1 h. Plasmids and linear polyethylenimine (PEI; MW = 25000, Polysciences) were premixed and incubated at room temperature for 25 min in the following amounts per plate: 2 mL of opti-MEM (GIBCO), 3 μg of pRTR2, 3 μg of pVSVG, 9 μg of p4.1R, 15 μg of pLenti-CaMKII-TRPV1-p2A-mCherry-WPRE or pLenti-CaMKII-mCherry-WPRE, and 90 mg of PEI and incubated at room temperature for 25 min. The transfection mixture was added to each plate (2 mL) and incubated at 37 °C for 6–18 h. The culture medium was then exchanged with 10 mL of fresh and prewarmed DMEM with 10% FBS. 48–72 h later, the culture medium was collected in 50 mL centrifuge tubes. The cell debris were removed by centrifugation at 3000 rpm for 5 min at 4 °C. The lentiviral medium was filtered with a 0.45 μm filter and stored at 4 °C before concentration. The approximate titer of lentivirus was evaluated using a lentiviral titration kit (Lenti-X GoStix Plus; ClonTech). The lentiviral medium was transferred to 50 mL centrifuge tubes, and 7 mL of 10% sucrose in PBS (Corning) was slowly added into the bottom of each tube. Lentivirus was pelleted by centrifugation at 11,000×g for 4 h at 4 °C.[61] After removal of the supernatant and drying of the centrifuge tubes, the lentivirus pellets were resuspended in PBS at 0.1%, the original volume of the lentiviral medium. The titer of lentivirus was approximated by a lentiviral titration kit (Lenti-X GoStix Plus; ClonTech)

with serial dilutions. The concentrated lentivirus was aliquoted and stored at −80 °C in a freezer until use.

Stereotactic Surgery and Device Implantation.

Eight-week-old male BL6C/57 mice (Jackson, BL6C/57, #000664) were anesthetized with 1–2% isoflurane and placed on a heat pad in a stereotaxic head frame (Kopf) and immediately injected subcutaneously with buprenorphine-slow release (ZooPharm, 1.0 mg/kg). After creation of a midline incision along the scalp, a craniotomy was performed using a rotary tool (Dremel Micro 8050) and a carbon steel burr (Heisinger, 19007-05). Implants were flushed with sterile PBS, fastened to the stereotaxic cannula holder, and connected to a Hamilton syringe (10 μL, World Precision Instruments). Concentrated lentivirus (>10^9 transducing units/mL for Lenti-CaMKIIα::TRPV1-p2A-mCherry or Lenti-CaMKIIα::mCherry) was loaded into a microfluidic channel, and the device was lowered into the skull (coordinates from bregma, in mm: ML: ±0.5, DV: −4.35, AP: −3.3). The virus solution (2 μL total) was slowly injected (flow rate: 75 nL/min), while the device was cemented to the skull using first C&B-Metabond adhesive cement (Parkell) and then dental cement (jet Set-4) to encase the device. After completion of the injection, the device remained attached to the Hamilton syringe for at least 10 min before being detached. The incision was then closed with sutures, and the mouse was given a subcutaneous injection of carprofen (5 mg/kg) and sterile Ringer's solution (0.6 mL) prior to recovery on a heat pad. For 3 days postimplantaion, mice were single-housed and closely monitored for signs of overall health. They were given Carprofen injections (0.6 mL, 0.25 mg/mL in sterile Ringer's solution) as necessary. After recovery, mice remained single-housed and were not used for experiments if they experienced symptoms of decreased health.

Injection for c-Fos Quantification.

Six to eight weeks following device implantation (above), mice were anesthetized with 2% isoflurane, and the microfluidic channels were flushed with compound sterile PBS 3x with a Hamilton syringe and 26G needle. The device was connected via mini-EVA tubing (McMaster, 1883T1) to a Hamilton syringe that had been pre-filled with the compound solution. The compound solution (3 μM total volume) was injected (600 nL/min), and for *red*-AzCA-4 injections, 420 or 565 nm irradiation was applied (2 Hz, 50% duty cycle) for 40 min (as described above). The animal was kept under anesthesia for a total of 90 min after the beginning of the injection to allow for c-Fos expression and then deeply anesthetized by Fatal-plus injection (0.075 mL of 97.5 mg/mL solution in NaCl) followed by a standard transcardial perfusion using PBS (50 mL) followed by PFA (Electron Microscopy Sciences, 50 mL, 4% in PBS).

Immunofluorescence Staining.

For immunofluorescence in cultured neurons, the coverslips were fixed with 4% PFA (Electron Microscopy Sciences, 190107) in PBS buffer for 20 min at room temperature and then washed out for 5 min with PBS. Coverslips were permeabilized with 0.2% Triton X-100 (Fisher Scientific, BP151-100) for 1 min and then washed with PBS for (3 × 5 min washes). The coverslips were then transferred to a new 24-well plate (Corning) and incubated in a blocking buffer (0.02% Triton X100 + 5% normal donkey serum [NDS] in

PBS) for 1 h at room temperature on an orbital shaker (100 rpm). The coverslips were then incubated in a primary antibody solution (1:300 dilution anti-NeuN antibody [Abcam ab177487], 0.02% Triton X100, 5% NDS in PBS). The plate was sealed with parafilm (Pechiney plastic) and incubated overnight (12–14 h) in the dark at room temperature on the orbital shaker. The coverslips were washed with PBS (3 × 5 min washes) on the shaker at room temperature and then transferred to the secondary antibody solution (1:1000 donkey anti-rabbit 488 secondary [Life Technologies A21206], 0.02% Triton X100, 5% NDS) and incubated for 1 h in the dark at room temperature on the shaker. The coverslips were again washed with PBS (3 × 5 min washes) and then incubated in the dark with a 2-[4-(aminoiminomethyl)phenyl]-1H-indole-6-carboximidamide hydrochloride (DAPI) solution (1:50000 dilution, from 5 mg/mL DMSO stock in PBS) for 10 min on the shaker. The coverslips were washed with Sudan Black (Sigma-Aldrich, MKCG8561) for 3 × 5 min washes (0.2 mg/mL in 70% EtOH) and washed with deionized water (2 × 5 min washes). Coverslips were then mounted on a microscope slide (VWR Superfrost Plus Micro Slide, 75 × 25 × 1 mm, 48311-703). The coverslips were covered with a mounting solution (Fluoromount), covered with a coverglass (VWR, 24 × 60 mm, 16004-096), and then stored in the dark at room temperature overnight before imaging.

For fixed brain slice immunofluorescence, mice were euthanized by standard transcardial perfusion using 4% PFA (PFA, Electron Microscopy Sciences) in PBS. After extraction, the brains were soaked in 4% PFA in the dark overnight at 4 °C. The brains were washed with PBS (3 × 15 mL for 15 min) and sectioned appropriately, and coronal or sagittal slices (60 μm thickness) were prepared with a vibratome (Leica VT1000S) with a FEATHER razor blade (Electron Microscopy Sciences, 72002) in ice-cold PBS buffer. The slices were stored in the dark in PBS buffer at 4 °C until staining. The slices were transferred to a Netwell insert (Corning, 3478) and then incubated in permeabilization/blocking buffer (0.3% Triton X100 + 3% normal donkey serum [NDS] in PBS) in a standard 12-well plate (Cellstar, 665180) for 1 h at room temperature in the dark on an orbital shaker (100 rpm). The slices were then transferred to the primary antibody solution (2 mL total volume, 1:1000 dilution primary antibody, 3% NDS in PBS). The plate was sealed with parafilm (Pechiney plastic) and incubated overnight (12–14 h) in the dark at room temperature on the shaker. The slices were washed with PBS (3 × 2 mL, 20 min each) on the shaker in the dark at room temperature, then transferred to the secondary antibody solution (2 mL total volume in PBS), and incubated for 2 h in the dark at room temperature on the shaker. The slices were again washed with PBS (3 × 2 mL, 20 min each) and then incubated in the dark with a DAPI solution (1:50000 dilution, from 5 mg/mL DMSO stock in PBS, 2 mL total volume) for 45 min on the shaker. The slices were again washed with PBS (2 × 2 mL, 20 min each) and then mounted on a cover slide (VWR Superfrost Plus Micro Slide, 75 × 25 × 1 mm, 48311-703). The slices were covered with a mounting solution (Fluoromount), covered with a coverglass (VWR, 24 × 60 mm, 16004-096), and then stored in the dark at room temperature overnight.

Confocal Microscopy.

Live-cell fluorescent Ca^{2+} imaging in cultured hippocampal neurons (DIV 10–14) was performed on a dual scanner Olympus Fluoview 1200 with a 20× objective (Olympus) at 37 °C in 5% CO_2. Cells were first loaded with Fluo-4-AM (2 μM, ThermoFisher, F14201) in

Neurobasal A+ media for 30 min and then washed twice with an imaging buffer (250 μL). Fluo-4 was excited at 488 nm at low laser power (<3%), and the emission was collected from 500–550 nm. Photoswitching was generated by 375 nm laser irradiation at 100% laser power and triggered using the quench function in the Olympus software. The fluorescence intensity data was extracted in ImageJ (NIH) and processed/plotted in MATLAB.

Fluorescence images in fixed and mounted sagittal brain slices were acquired on an Olympus Fluoview FV1000 laser-scanning confocal microscope with a 20× objective (oil, NA = 0.85) and 60× (oil, NA = 1.42) objective. For images of each brain region, serial z-stack images with a step size of 4 μm were acquired. The center of the frame was positioned at the following: VTA - ML: ±0.48 mm, DV: −4.4 mm, AP: −3.3 mm; mPFC - ML: ±0.36 mm, DV: −2.5 mm, AP: +1.5 mm; NAc - ML: ±0.72 mm, DV: −3.9 mm, AP: −1.25 mm.[62] Coordinates were determined for each region using the Alan Brain Atlas. DAPI was excited using a 405 nm laser with emission light collected between 425 and 460 nm. Alexa Fluor 488 imaging was excited using a 473 nm laser with emission light collected between 485 and 515 nm. mCherry was visualized using a 559 nm laser with collected emission light between 575 and 675 nm.

Following imaging, the data was analyzed with a custom MATLAB script (available on request) and ImageJ (NIH), which directly processed output.oib files without user intervention to generate the z-stacks and quantify the percentage of c-Fos positive cells. Statistical significance was assessed in MATLAB using a two-sample *t* test. All imaging and analysis were blinded with respect to the experimental conditions.

Conditioned Place Preference.

Conditioned place preference (CPP) experiments were performed in a home-built three chamber box with dimensions 21 × 25, 21 × 20, and 21 × 25 cm for the left, center, and right chambers, respectively. The base was fabricated out of white polyethylene sheets (McMaster, 8752K315) to facilitate cleaning between trials. The left chamber had a white plastic floor with punched holes (2.38 mm diameter, 25% open area) (McMaster #9293T67) and walls with a magenta polka-dot pattern. The center chamber had a flat Teflon floor (McMaster) with no wall pattern. The right chamber had a floor made of plastic bars (1/8 in. diameter, 7.62 mm spacing) (McMaster, 8658K47) and diagonal green bars on the walls. The walls and doors to separate the chambers were fabricated out of transparent polycarbonate (McMaster). A webcam (Logitech), microinjector pump (World Precision Instruments, Micro4, UMC4), and the rotary joint of the optical waveguide (Thorlabs, RJPSF2) were mounted directly above the center chamber. Experiments were performed in a room with normal fluorescent lighting, and the light intensity was kept constant across the box and consistent throughout all experimental days. Video recording of all trial days (days 1–4) were recorded using the webcam software (Logitech). The absolute position of the mouse in the box was determined using a custom python script (available on request), and the percent time spent in each chamber of the box was calculated using MATLAB (script available on request). The first 30 min of the video were used for quantification, and the time in either the holes vs bars chamber were scored as a percentage. Preconditioning was performed for 3 days prior to the behavioral experiments to habituate

them to being restrained and attached to optical/fluid delivery cables. Additionally, the microfluidic channels were gently washed with 3 × 10 μL sterile PBS to remove any excess salt or blood which may be clogging the channels. This flushing step was repeated at the beginning of each experimental day to ensure any residual compound solution or salts remaining in the tubes were removed. No pressure was applied, so these washes did not result in fluid injection into the brain. The experimental paradigm for the 4-day conditioned place preference (CPP) test is as follows:

Day 1, Pretest: The microfluidic channel was flushed with 3 × 10 μL washes of PBS buffer, and the device was connected to an optical fiber and the injection tubing. The mouse was then placed in the center chamber with closed doors. The doors were then removed, and the mouse was left to explore the entire box for 45 min.

Day 2, Condition 1: Microfluidic channels were flushed with 3 × 10 μL washes of the compound solution (0.1% DMSO or 1 μM *red*-AzCA-4), and the device was connected to the optical fiber and injection tubing. The mouse was placed in either the holes or bars chamber, which was sealed by the transparent door. To minimize potential bias toward a particular chamber, the mice were evenly distributed between holes or bars on the second and third day of conditioning. The trial was initiated at the start of the injection (3 μL at 600 nL/min), and the mouse was kept in the conditioning chamber for 45 min. For trials with *red*-AzCA-4, 420 nm light was applied (7.6 mW/mm^2 on average) at 2 Hz at 50% duty cycle. After the trial, the channels were again washed with 3 × 10 μL sterile PBS before the mice were returned to the animal facility overnight.

Day 3, Condition 2: The procedure for day 3 was the same as day 2, except mice were placed in the opposite chamber as Day 2. On this day, the mice which previously received the vehicle control received a 10 μM CAP injection. The mice which previously received the *red*-AzCA-4 with blue light received the same dose of *red*-AzCA-4, except with 565 nm irradiation (2 Hz at 50% duty cycle, 8.1 mW/mm^2 on average).

Day 4, Post-Test: Identical to the procedure described above for day 1.

Quantification and Statistical Analysis.

Unless otherwise described, all data is presented as mean ± SEM. For Ca^{2+} imaging experiments, *n* is the number of measurements made (individual cells), and the number of individual experiments (biological replicates) is described in the figure caption. Statistical significance was assessed using MATLAB (Mathworks) and Excel (Microsoft). For the comparison between two groups in immunohistochemistry analyses, Student's two-sample *t* test (two-sided) was used, with significance threshold placed at $*P < 0.05$. For the comparison between two groups in behavior assays, a Wilcoxon signed-rank test was used, with significance thresholds placed at * = $0.02 < P < 0.05$; ns = not significant = $P > 0.2$.

Supplementary Material

Refer to Web version on PubMed Central for supplementary material.

ACKNOWLEDGMENTS

The authors thank Prof. Dirk Trauner for his input on this study.

Funding

This work was funded in part by the National Institute of Neurological Disorders and Stroke (5R01NS086804), the National Institutes of Health (NIH) BRAIN Initiative (1R01MH111872), the National Science Foundation (NSF) Center for Neurotechnology (EEC-1028725), and the McGovern Institute for Brain Research. This work made use of the MIT MRSEC Shared Experimental Facilities under award number DMR-14-19807 from the NSF. Additional support was provided by the US Army Research Laboratory and the US Army Research Office through the Institute for Soldier Nanotechnologies under contract number W911NF-13-D-000. J.A.F. acknowledges the Vollum Institute Fellowship for financial support. M.J.A. is a recipient of the Friends of McGovern Graduate Fellowship.

ABBREVIATIONS

CAP	capsaicin
COC	cyclic olefin copolymer
CPP	conditioned place preference
EVA	ethyl vinyl acetate
GPCR	G protein-coupled receptor
LED	light-emitting diode
mCh	mCherry
mPFC	medial prefrontal cortex
NAc	nucleus accumbens
PC	polycarbonate
TDP	thermal drawing process
TRPV1	transient receptor potential vanilloid family member 1-capsaicin receptor
VTA	ventral tegmental area

REFERENCES

(1). Rajasethupathy P, Ferenczi E, and Deisseroth K (2016) Targeting Neural Circuits. Cell 165 (3), 524–534. [PubMed: 27104976]

(2). Mondoloni S, Durand-De Cuttoli R, and Mourot A (2019) Cell-Specific Neuropharmacology. Trends Pharmacol. Sci 40 (9), 696–710. [PubMed: 31400823]

(3). Paoletti P, Ellis-Davies GCR, and Mourot A (2019) Optical Control of Neuronal Ion Channels and Receptors. Nat. Rev. Neurosci 20 (9), 514–532. [PubMed: 31289380]

(4). Zemelman BV, Lee GA, Ng M, and Miesenböck G (2002) Selective Photostimulation of Genetically ChARGed Neurons. Neuron 33 (1), 15–22. [PubMed: 11779476]

(5). Durand-de Cuttoli R, Chauhan PS, Pétriz A, Faure P, Mourot A, and Ellis-Davies GCR (2020) Optofluidic Control of Rodent Learning Using Cloaked Caged Glutamate. Proc. Natl. Acad. Sci. U. S. A 117 (12), 6831–6835. [PubMed: 32152102]

(6). Mourot A, Fehrentz T, Le Feuvre Y, Smith CM, Herold C, Dalkara D, Nagy F, Trauner D, and Kramer RH (2012) Rapid Optical Control of Nociception with an Ion-Channel Photoswitch. Nat. Methods 9 (4), 396–402. [PubMed: 22343342]

(7). Kienzler MA, and Isacoff EY (2017) Precise Modulation of Neuronal Activity with Synthetic Photoswitchable Ligands. Curr. Opin. Neurobiol 45, 202–209. [PubMed: 28690101]

(8). Broichhagen J, Frank JA, and Trauner D (2015) A Roadmap to Success in Photopharmacology. Acc. Chem. Res 48 (7), 1947–1960. [PubMed: 26103428]

(9). Hüll K, Morstein J, and Trauner D (2018) In Vivo Photopharmacology. Chem. Rev 118 (21), 10710–10747. [PubMed: 29985590]

(10). Levitz J, Broichhagen J, Leippe P, Konrad D, Trauner D, and Isacoff EY (2017) Dual Optical Control and Mechanistic Insights into Photoswitchable Group II and III Metabotropic Glutamate Receptors. Proc. Natl. Acad. Sci. U. S. A 114 (17), E3546–E3554. [PubMed: 28396447]

(11). Borowiak M, Nahaboo W, Reynders M, Nekolla K, Jalinot P, Hasserodt J, Rehberg M, Delattre M, Zahler S, Vollmar A, Trauner D, and Thorn-Seshold O (2015) Photoswitchable Inhibitors of Microtubule Dynamics Optically Control Mitosis and Cell Death. Cell 162 (2), 403–411. [PubMed: 26165941]

(12). Urban P, Pritzl SD, Konrad DB, Frank JA, Pernpeintner C, Roeske CR, Trauner D, and Lohmüller T (2018) Light-Controlled Lipid Interaction and Membrane Organization in Photolipid Bilayer Vesicles. Langmuir 34 (44), 13368–13374. [PubMed: 30346771]

(13). Difrancesco ML, Lodola F, Colombo E, Maragliano L, Bramini M, Paternò GM, Baldelli P, Serra MD, Lunelli L, Marchioretto M, Grasselli G, Cimò S, Colella L, Fazzi D, Ortica F, Vurro V, Eleftheriou CG, Shmal D, Maya-Vetencourt JF, Bertarelli C, Lanzani G, and Benfenati F (2020) Neuronal Firing Modulation by a Membrane-Targeted Photoswitch. Nat. Nanotechnol 15, 296. [PubMed: 32015505]

(14). Kol M, Williams B, Toombs-Ruane H, Franquelim HG, Korneev S, Schroeer C, Schwille P, Trauner D, Holthuis JCM, and Frank JA (2019) Optical Manipulation of Sphingolipid Biosynthesis Using Photoswitchable Ceramides. eLife 8, No. e43230.

(15). Broichhagen J, Cork SC, Frank JA, Marchetti P, Broichhagen J, Scho M, Bugliani M, Shapiro AMJ, Trapp S, Rutter GA, Hodson DJ, and Trauner D (2014) Optical Control of Insulin Release Using a Photoswitchable Sulfonylurea. Nat. Commun 5, 6116.

(16). Banghart M, Borges K, Isacoff E, Trauner D, and Kramer RH (2004) Light-Activated Ion Channels for Remote Control of Neuronal Firing. Nat. Neurosci 7 (12), 1381–1386. [PubMed: 15558062]

(17). Tochitsky I, Banghart MR, Mourot A, Yao JZ, Gaub B, Kramer RH, and Trauner D (2012) Optochemical Control of Genetically Engineered Neuronal Nicotinic Acetylcholine Receptors. Nat. Chem 4 (2), 105–111. [PubMed: 22270644]

(18). Wyart C, Bene Del F, Warp E, Scott EK, Trauner D, Baier H, and Isacoff EY (2009) Optogenetic Dissection of a Behavioural Module in the Vertebrate Spinal Cord. Nature 461 (7262), 407–410. [PubMed: 19759620]

(19). Cabré G, Garrido-Charles A, Moreno M, Bosch M, Porta-De-La-Riva M, Krieg M, Gascón-Moya M, Camarero N, Gelabert R, Lluch JM, Busqué F, Hernando J, Gorostiza P, and Alibés R (2019) Rationally Designed Azobenzene Photoswitches for Efficient Two-Photon Neuronal Excitation. Nat. Commun 10, 907. [PubMed: 30796228]

(20). Zussy C, Gómez-Santacana X, Rovira X, De Bundel D, Ferrazzo S, Bosch D, Asede D, Malhaire F, Acher F, Giraldo J, Valjent E, Ehrlich I, Ferraguti F, Pin JP, Llebaria A, and Goudet C (2018) Dynamic Modulation of Inflammatory Pain-Related Affective and Sensory Symptoms by Optical Control of Amygdala Metabotropic Glutamate Receptor 4. Mol. Psychiatry 23 (3), 509–520. [PubMed: 27994221]

(21). Durand-de Cuttoli R, Mondoloni S, Marti F, Lemoine D, Nguyen C, Maskos U, Trauner D, Kramer RH, Faure P, and Mourot A (2018) Manipulating Midbrain Dopamine Neurons and Reward-Related Behaviors with Light- Controllable Nicotinic Acetylcholine Receptors. eLife 7, No. e37487.

(22). Acosta-Ruiz A, Gutzeit VA, Skelly MJ, Meadows S, Lee J, Orr AG, Pleil K, Broichhagen J, and Levitz J (2020) Branched Photoswitchable Tethered Ligands Enable Ultra-Efficient

Optical Control and Detection of Class C G Protein-Coupled Receptors. Neuron 105, 446–463. [PubMed: 31784287]

(23). Park S, Loke G, Fink Y, and Anikeeva P (2019) Flexible Fiber-Based Optoelectronics for Neural Interfaces. Chem. Soc. Rev 48 (6), 1826–1852. [PubMed: 30815657]

(24). Jeong JW, McCall JG, Shin G, Zhang Y, Al-Hasani R, Kim M, Li S, Sim JY, Jang KI, Shi Y, Hong DY, Liu Y, Schmitz GP, Xia L, He Z, Gamble P, Ray WZ, Huang Y, Bruchas MR, and Rogers JA (2015) Wireless Optofluidic Systems for Programmable In Vivo Pharmacology and Optogenetics. Cell 162 (3), 662–674. [PubMed: 26189679]

(25). Canales A, Jia X, Froriep UP, Koppes RA, Tringides CM, Selvidge J, Lu C, Hou C, Wei L, Fink Y, and Anikeeva P (2015) Multifunctional Fibers for Simultaneous Optical, Electrical and Chemical Interrogation of Neural Circuits in Vivo. Nat. Biotechnol 33 (3), 277–284. [PubMed: 25599177]

(26). Shin H, Son Y, Chae U, Kim J, Choi N, Lee HJ, Woo J, Cho Y, Yang SH, Lee CJ, and Cho IJ (2019) Multifunctional Multi-Shank Neural Probe for Investigating and Modulating Long-Range Neural Circuits in Vivo. Nat. Commun 10, 3777. [PubMed: 31439845]

(27). Kampasi K, English DF, Seymour J, Stark E, McKenzie S, Vöröslakos M, Buzsáki G, Wise KD, and Yoon E (2018) Dual Color Optogenetic Control of Neural Populations Using Low-Noise, Multishank Optoelectrodes. Microsystems Nanoeng. 4 (1), 10.

(28). Minev I, Musienko P, Hirsch A, Barraud Q, Wenger N, Moraud E, Gandar J, Capogrosso M, Milekovic T, Asboth L, Torres R, Vachicouras N, Liu Q, Pavlova N, Duis S, Larmagnac A, Voros J, Micera S, Sui Z, Courtine G, and Lacour S (2015) Electronic Dura Mater for Long-Term Multimodal Neural Interfaces. Science 347 (6218), 159–163. [PubMed: 25574019]

(29). Petit-Pierre G, Bertsch A, and Renaud P (2016) Neural Probe Combining Microelectrodes and a Droplet-Based Microdialysis Collection System for High Temporal Resolution Sampling. Lab Chip 16 (5), 917–924. [PubMed: 26864169]

(30). Kuzum D, Takano H, Shim E, Reed JC, Juul H, Richardson AG, De Vries J, Bink H, Dichter MA, Lucas TH, Coulter DA, Cubukcu E, and Litt B (2014) Transparent and Flexible Low Noise Graphene Electrodes for Simultaneous Electrophysiology and Neuroimaging. Nat. Commun 5, 5259. [PubMed: 25327632]

(31). Lu L, Gutruf P, Xia L, Bhatti DL, Wang X, Vazquez-Guardado A, Ning X, Shen X, Sang T, Ma R, Pakeltis G, Sobczak G, Zhang H, Seo D, Xue M, Yin L, Chanda D, Sheng X, Bruchas MR, and Rogers JA (2018) Wireless Optoelectronic Photometers for Monitoring Neuronal Dynamics in the Deep Brain. Proc. Natl. Acad. Sci. U. S. A 115 (7), E1374–E1383. [PubMed: 29378934]

(32). Park S, Guo Y, Jia X, Choe HK, Grena B, Kang J, Park J, Lu C, Canales A, Chen R, Yim YS, Choi GB, Fink Y, and Anikeeva P (2017) One-Step Optogenetics with Multifunctional Flexible Polymer Fibers. Nat. Neurosci 20 (4), 612–619. [PubMed: 28218915]

(33). Lu C, Park S, Richner TJ, Derry A, Brown I, Hou C, Rao S, Kang J, Moritz CT, Fink Y, and Anikeeva P (2017) Flexible and Stretchable Nanowire-Coated Fibers for Optoelectronic Probing of Spinal Cord Circuits. Sci. Adv 3, No. e1600955.

(34). Canales A, Park S, Kilias A, and Anikeeva P (2018) Multifunctional Fibers as Tools for Neuroscience and Neuroengineering. Acc. Chem. Res 51 (4), 829–838. [PubMed: 29561583]

(35). Konrad DB, Frank JA, and Trauner D (2016) Synthesis of Redshifted Azobenzene Photoswitches by Late-Stage Functionalization. Chem. - Eur. J 22 (13), 4364–4368. [PubMed: 26889884]

(36). Szallasi A, Cortright DN, Blum CA, and Eid SR (2007) The Vanilloid Receptor TRPV1:10 Years from Channel Cloning to Antagonist Proof-of-Concept. Nat. Rev. Drug Discovery 6 (5), 357–372. [PubMed: 17464295]

(37). Caterina MJ, Schumacher M. a, Tominaga M, Rosen T. a, Levine JD, and Julius D. (1997) The Capsaicin Receptor: A Heat-Activated Ion Channel in the Pain Pathway. Nature 389 (6653), 816–824. [PubMed: 9349813]

(38). Frank JA, Moroni M, Moshourab R, Sumser M, Lewin GR, and Trauner D (2015) Photoswitchable Fatty Acids Enable Optical Control of TRPV1. Nat. Commun 6 (May), 7118. [PubMed: 25997690]

(39). Dong M, Babalhavaeji A, Samanta S, Beharry AA, and Woolley GA (2015) Red-Shifting Azobenzene Photoswitches for in Vivo Use. Acc. Chem. Res 48, 2662–2670. [PubMed: 26415024]

(40). Samanta S, Beharry A. a., Sadovski O, McCormick TM, Babalhavaeji A, Tropepe V, and Woolley GA (2013) Photoswitching Azo Compounds in Vivo with Red Light. J. Am. Chem. Soc 135 (26), 9777–9784. [PubMed: 23750583]

(41). Kim JH, Lee S, Li L, Park H, Park J, Lee KY, Kim M, Shin BA, and Choi S (2011) High Cleavage Efficiency of a 2A Peptide Derived from Porcine Teschovirus-1 in Human Cell Lines, Zebrafish and Mice. PLoS One 6 (4), No. e18556.

(42). Chen R, Romero G, Christiansen MG, Mohr A, and Anikeeva P (2015) Wireless Magnetothermal Deep Brain Stimulation. Science 347, 1477–1480. [PubMed: 25765068]

(43). Wolf HK, Buslei R, Schmidt-Kastner R, Schmidt-Kastner PK, Pietsch T, Wiestler OD, and Blümcke I (1996) NeuN: A Useful Neuronal Marker for Diagnostic Histopathology. J. Histochem. Cytochem 44 (10), 1167–1171. [PubMed: 8813082]

(44). Qu Y, Nguyen-Dang T, Page AG, Yan W, Das Gupta T, Rotaru GM, Rossi RM, Favrod VD, Bartolomei N, and Sorin F (2018) Superelastic Multimaterial Electronic and Photonic Fibers and Devices via Thermal Drawing. Adv. Mater 30 (27), 1707251.

(45). Bromberg-Martin ES, Matsumoto M, and Hikosaka O (2010) Dopamine in Motivational Control: Rewarding, Aversive, and Alerting. Neuron 68 (5), 815–834. [PubMed: 21144997]

(46). Björklund A, and Dunnett SB (2007) Dopamine Neuron Systems in the Brain: An Update. Trends Neurosci. 30 (5), 194–202. [PubMed: 17408759]

(47). Russo SJ, and Nestler EJ (2013) The Brain Reward Circuitry in Mood Disorders. Nat. Rev. Neurosci 14 (9), 609–625. [PubMed: 23942470]

(48). Liu X, Liu Y, Zhong P, Wilkinson B, Qi J, Olsen CM, Bayer KU, and Liu QS (2014) CaMKII Activity in the Ventral Tegmental Area Gates Cocaine-Induced Synaptic Plasticity in the Nucleus Accumbens. Neuropsychopharmacology 39 (4), 989–999. [PubMed: 24154664]

(49). Jackson KJ, Muldoon PP, Walters C, and Damaj MI (2016) Neuronal Calcium/Calmodulin-Dependent Protein Kinase-II Mediates Nicotine Reward in the Conditioned Place Preference Test in Mice. Behav. Pharmacol 27 (1), 50–56. [PubMed: 26292186]

(50). Güler AD, Rainwater A, Parker JG, Jones GL, Argilli E, Arenkiel BR, Ehlers MD, Bonci A, Zweifel LS, and Palmiter RD (2012) Transient Activation of Specific Neurons in Mice by Selective Expression of the Capsaicin Receptor. Nat. Commun 3 (746), 1749.

(51). Dragunow M, and Faull R. (1989) The Use of C-Fos as a Metabolic Marker in Neuronal Pathway Tracing. J. Neurosci. Methods 29 (3), 261–265. [PubMed: 2507830]

(52). Tsai H-C, Zhang F, Adamantidis A, Stuber GD, Bonci A, de Lecea L, and Deisseroth K (2009) Phasic Firing in Dopaminergic Neurons Is Sufficient for Behavioral COnditioning. Science 324, 1080–1084. [PubMed: 19389999]

(53). Tzschentke TM (2007) Measuring Reward with the Conditioned Place Preference (CPP) Paradigm: Update of the Last Decade. Addict. Biol 12 (3–4), 227–462. [PubMed: 17678505]

(54). Deal WJ, Erlanger BF, and Nachmansohn D (1969) Photoregulation of Biological Activity By Photochromic Reagents, III. Photoregulation of Bioelectricity By Acetylcholine Receptor Inhibitors. Proc. Natl. Acad. Sci. U. S. A 64 (4), 1230–1234. [PubMed: 5271749]

(55). Lester HA, Krouse ME, Nass MM, Wassermann NH, and Erlanger BF (1980) A Covalently Bound Photoisomerizable Agonist: Comparison with Reversibly Bound Agonists at Electrophorus Electroplaques. J. Gen. Physiol 75, 207–232. [PubMed: 6246192]

(56). Spencer KC, Sy JC, Ramadi KB, Graybiel AM, Langer R, and Cima MJ (2017) Characterization of Mechanically Matched Hydrogel Coatings to Improve the Biocompatibility of Neural Implants. Sci. Rep 7 (1), 1952. [PubMed: 28512291]

(57). Shin G, Gomez AM, Al-Hasani R, Jeong YR, Kim J, Xie Z, Banks A, Lee SM, Han SY, Yoo CJ, Lee JL, Lee SH, Kurniawan J, Tureb J, Guo Z, Yoon J, Park S Il, Bang SY, Nam Y, Walicki MC, Samineni VK, Mickle AD, Lee K, Heo SY, McCall JG, Pan T, Wang L, Feng X, Kim T. il, Kim JK, Li Y, Huang Y, Gereau RW, Ha JS, Bruchas MR, and Rogers JA (2017) Flexible Near-Field Wireless Optoelectronics as Subdermal Implants for Broad Applications in Optogenetics. Neuron 93 (3), 509–521.e3. [PubMed: 28132830]

(58). Park S. Il, Brenner DS, Shin G, Morgan CD, Copits BA, Chung HU, Pullen MY, Noh KN, Davidson S, Oh SJ, Yoon J, Jang KI, Samineni VK, Norman M, Grajales-Reyes JG, Vogt SK, Sundaram SS, Wilson KM, Ha JS, Xu R, Pan T, Kim T Il, Huang Y, Montana MC, Golden JP, Bruchas MR, Gereau RW, and Rogers JA (2015) Soft, Stretchable, Fully Implantable Miniaturized Optoelectronic Systems for Wireless Optogenetics. Nat. Biotechnol 33 (12), 1280–1286. [PubMed: 26551059]

(59). Zhang H, Gutruf P, Meacham K, Montana MC, Zhao X, Chiarelli AM, Vázquez-Guardado A, Norris A, Lu L, Guo Q, Xu C, Wu Y, Zhao H, Ning X, Bai W, Kandela I, Haney CR, Chanda D, Gereau RW, and Rogers JA (2019) Wireless, Battery-Free Optoelectronic Systems as Subdermal Implants for Local Tissue Oximetry. Sci. Adv 5 (3), No. eaaw0873.

(60). Westphal MV, Schafroth MA, Sarott RC, Imhof MA, Bold CP, Leippe P, Dhopeshwarkar A, Grandner JM, Katritch V, Mackie K, Trauner D, Carreira EM, and Frank JA (2017) Synthesis of Photoswitchable Δ^9 -Tetrahydrocannabinol Derivatives Enables Optical Control of Cannabinoid Receptor 1 Signaling. J. Am. Chem. Soc 139 (50), 18206–18212. [PubMed: 29161035]

(61). Jiang W, Hua R, Wei M, Li C, Qiu Z, Yang X, and Zhang C (2015) An Optimized Method for High-Titer Lentivirus Preparations without Ultracentrifugation. Sci. Rep 5, 13875. [PubMed: 26348152]

(62). Paxinos G, and Franklin K (2001) The Mouse Brain in Stereotaxic Coordinates, 2nd ed., Academic Press, San Diego, CA.

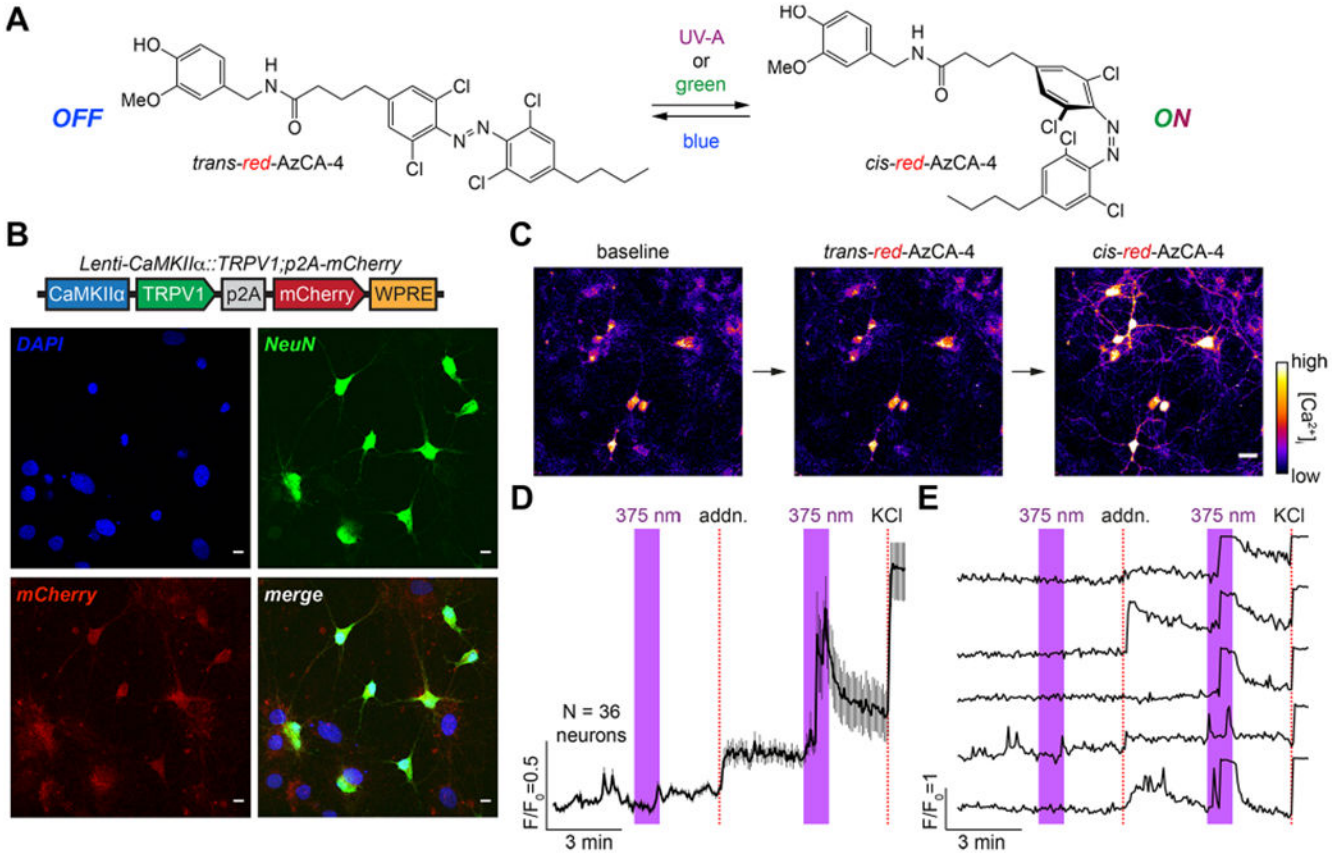

Figure 1.

red-AzCA-4 enables optical control of TRPV1-infected primary neurons. (**A**) Chemical structure of *red*-AzCA-4, which can be isomerized between its *cis*- and *trans*-isomers with UV-A/green and blue light, respectively. (**B**) Cultured rat hippocampal neurons were infected with a virus encoding for TRPV1 and mCherry under the CaMKIIα promoter. Immunofluorescence imaging showed that neurons (NeuN, green) were expressed as mCherry (red). Scale bar = 10 μm. (C–E) Fluorescent Ca^{2+} imaging of Fluo-4-loaded neurons showed that *red*-AzCA-4 (20 nM) stimulated $[Ca^{2+}]_i$. Displayed as (**C**) representative images. Scale bar = 25 μm, (**D**) average normalized Ca^{2+} levels over multiple cells (N = 36 neurons, 2 experiments, error bars = mean ± SEM), and (**E**) representative Ca^{2+} traces from five individual neurons.

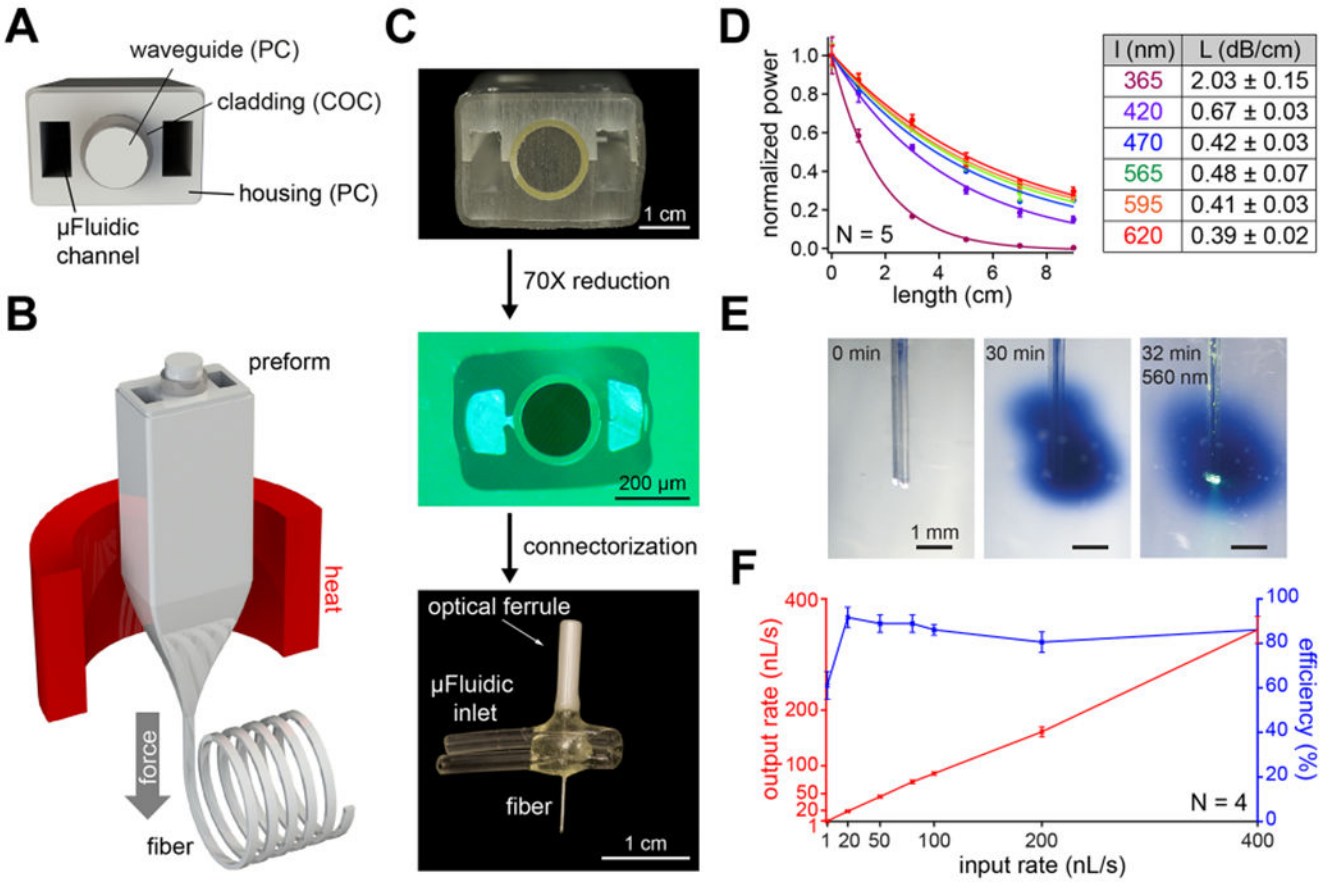

Figure 2.

Design and fabrication of a multifunctional fiber-based implant by thermal drawing. (**A**) Cross-section schematic of implants with two microfluidic channels and optical waveguide. (**B**) Schematic representing the thermal drawing process. (**C**) Cross-section of the preforms before thermal drawing (top). Cross-section of fibers after thermal drawing (middle). Fully connectorized device (bottom). (**D**) Optical loss calculation of the PC/COC optical waveguide across the visible spectrum ($N = 5$). (**E**) Injection of Trypan blue dye (2 μL over 30 min) into a phantom brain (0.6% agarose gel). 565 nm LED irradiation emerges from the device tip. (**F**) Output rate and efficiency following injection of 9 μL of water into a phantom brain using the microfluidic channel of 1 cm long multifunctional fiber-based neural implant ($N = 4$). Error bars = mean ± SEM.

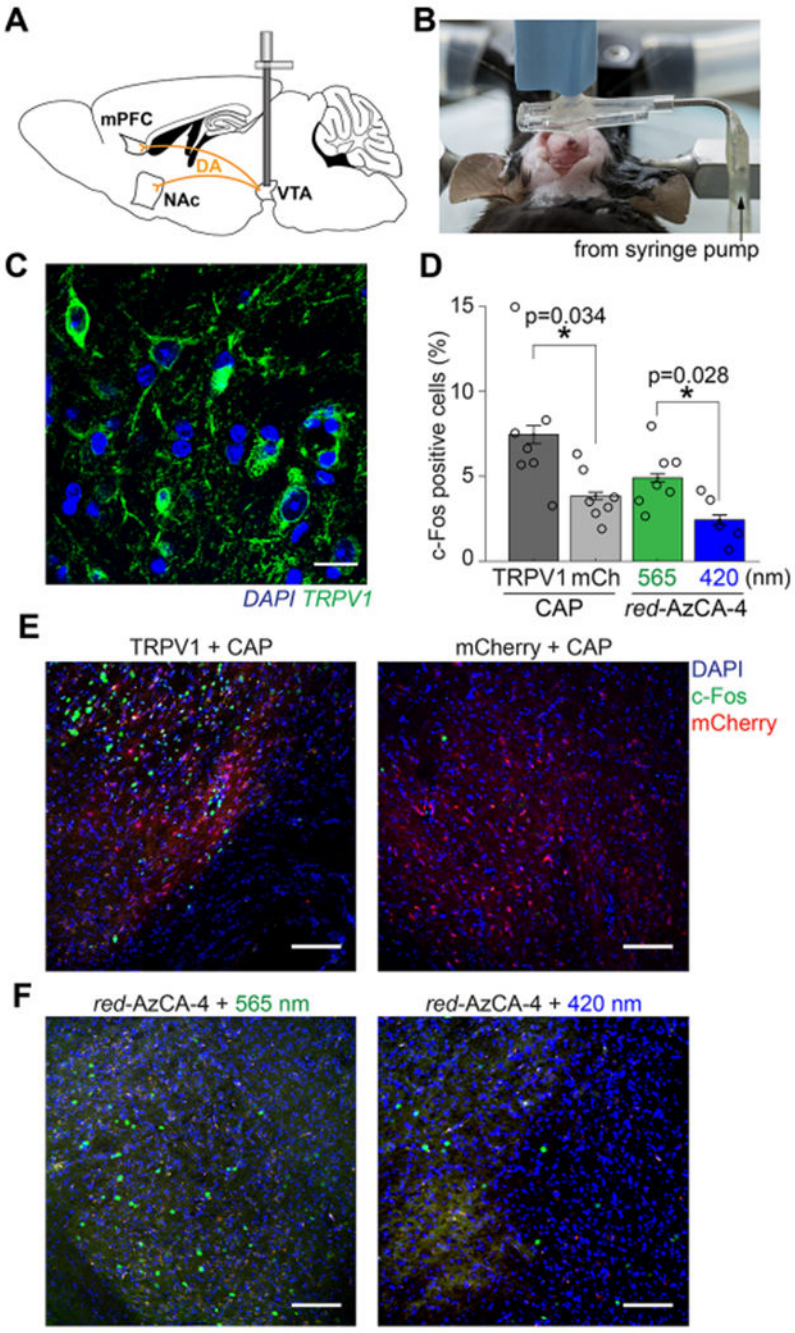

Figure 3.

In vivo chemogenetic stimulation of midbrain dopaminergic circuits. (**A**) Schematic of VTA dopamine projections to the mPFC and NAc. (**B**) Image displaying the craniotomy procedure while simultaneously injecting virus and implanting the probe. (**C**) Six weeks following viral injection and device implantation, immunofluorescence imaging using an anti-TRPV1 antibody confirmed TRPV1 expression (green) in the VTA. Brain slices were co-stained with the DAPI nuclear marker (blue). Scale bar = 10 μm. (**D**) Quantification of c-Fos expression in the VTA following injection of CAP or *red*-AzCA-4 (with 565 or 420

nm irradiation) over multiple animals (TRPV1 + CAP, $N = 7$; mCherry, $N = 7$; *red*-AzCA-4 + 565 nm light, $N = 7$; red-AzCA-4 + 420 nm light, $N = 5$). (**E**) Injection of CAP (10 μM) caused an increase in c-Fos expression (green nuclei) in the TRPV1-expressing VTA neurons (left panel) when compared to those expressing mCherry only (right panel). (**F**) Injection of *red*-AzCA-4 (1 μM) caused increased c-Fos expression in the VTA when paired with 565 nm light (left panel) as compared to 420 nm light (right panel). Scale bar = 100 μm. Error bars = mean ± SEM.

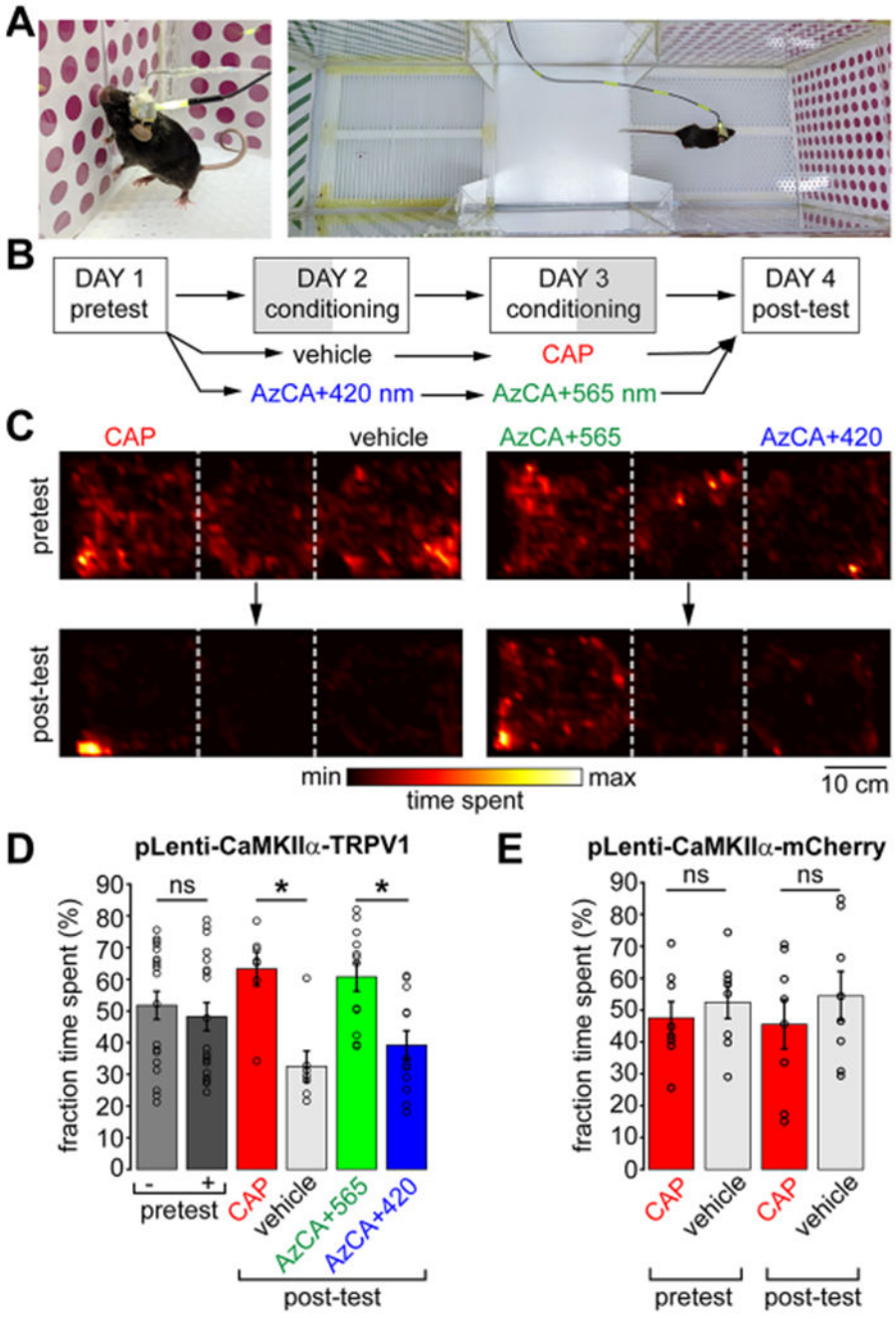

Figure 4.

red-AzCA-4 enables light-dependent control of reward behavior in freely moving animals. (**A**) Awake and freely moving mice were connected to a microfluidic pump and LEDs and subject to a CPP test. (**B**) Timeline of the 4-day CPP test. (**C**) Heatmaps depicting the relative time spent at each position in the box for a representative mouse during the pretest (top) and after conditioning (post-test, bottom) with CAP/vehicle (left) or *red*-AzCA-4 + 420/565 nm irradiation (right). (**D**) TRPV1-expressing mice did not have a preference for either chamber during the pretest day ($N = 19$). Mice preferred the chamber where

they received CAP over a vehicle control on the post-test day after conditioning ($N = 7$). Mice preferred the chamber where they received *cis-red*-AzCA-4 (green light) over *trans-red*-AzCA-4 (blue light) after their conditioning ($N = 12$). (**E**) Mice which only expressed mCherry and not TRPV1 did not develop a preference for the chamber associated with CAP delivery ($N = 8$). Error bars = mean ± SEM. * = $P < 0.05$; ns = not significant = $P > 0.05$.